INSTITUTE OF PHYSICS PUBLISHING SUPERCONDUCTOR SCIENCE AND TECHNOLOGY
Supercond. Sci. Technol. **19** (2006) 987–997 doi:10.1088/0953-2048/19/10/001

THELMA code electromagnetic model of ITER superconducting cables and application to the ENEA stability experiment

M Ciotti[1], A Nijhuis[2], P L Ribani[3], L Savoldi Richard[4] and R Zanino[4,5]

[1] Associazione EURATOM-ENEA sulla Fusione, 00044 Frascati, Italy
[2] Faculty of Science and Technology, University of Twente, 7500 AE Enschede, The Netherlands
[3] Dipartimento di Ingegneria Elettrica, Università di Bologna, 40136 Bologna, Italy
[4] Dipartimento di Energetica, Politecnico, 10129 Torino, Italy

E-mail: roberto.zanino@polito.it

Received 6 June 2006, in final form 10 July 2006
Published 21 August 2006
Online at stacks.iop.org/SUST/19/987

Abstract
The new THELMA code, including a thermal-hydraulic (TH) and an electro-magnetic (EM) model of a cable-in-conduit conductor (CICC), has been developed. The TH model is at this stage relatively conventional, with two fluid components (He flowing in the annular cable region and He flowing in the central channel) being particular to the CICC of the International Thermonuclear Experimental Reactor (ITER), and two solid components (superconducting strands and jacket/conduit). In contrast, the EM model is novel and will be presented here in full detail. The results obtained from this first version of the code are compared with experimental results from pulsed tests of the ENEA stability experiment (ESE), showing good agreement between computed and measured deposited energy and subsequent temperature increase.

(Some figures in this article are in colour only in the electronic version)

1. Introduction

Code development is a crucial issue towards the possibility of predicting superconducting magnet behaviour especially in the case of their utilization in large scale fusion devices, such as the International Thermonuclear Experimental Reactor (ITER) project, for the optimization of cost and performances. Testing of real magnets, even sub-size or sub-modules, may be extremely expensive and time consuming, so that it is necessary to proceed on a double track both on the side of experiments and of developing, implementing and validating computational tools.

Cable-in-conduit conductors (CICCs) have been designed for the ITER magnets. The superconducting material will be Nb_3Sn for the central solenoid and toroidal field coils, and NbTi for the poloidal field coils. Recent results on the major world wide experiments such as the ITER model coils and short samples [1–7] show that the predictability of the coil behaviour is still not completely achieved and some phenomena, such as current distribution and (for Nb_3Sn) local strain, can play a very important role in the magnet performances and should be introduced in the simulation codes.

A large effort has been devoted in recent years to the development of codes to analyse current distribution and AC losses in superconducting multi-strand cables. The main difference between the developed codes is the approach used to describe the electromagnetic phenomena: a lumped parameter circuit description [8–14] or a distributed parameter circuit

[5] Author to whom any correspondence should be addressed.

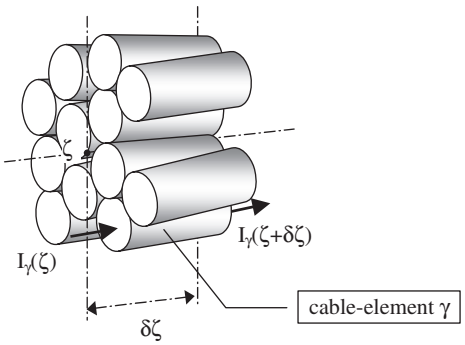

Figure 1. Schematic view of a segment of the cable in the case each cable element CE represents a strand.

description [15–17]. Each approach has advantages and disadvantages, which will not be discussed in this paper. The approach used here is the distributed parameters one, which seems to have some advantages when long, real size cable are analysed and coupling with thermal-hydraulic phenomena needs to be included.

In the framework of the European Fusion Development Agreement (EFDA) activity towards the comprehensive modelling of the ITER CICC, the new code THELMA (thermal-hydraulic-electro-magnetic), has been developed in a collaboration among Italian universities, under the coordination of ENEA Frascati. The thermal-hydraulic description is coupled with an electro-magnetic one, including both the cable and the joints. In this paper we present the model implemented in THELMA and the results obtained by the code are compared with a subset of the experimental results from the ENEA stability experiment (ESE), based on a sub-size CICC. While THELMA was already applied to the analysis of pulsed tests in a short (∼3 m) ITER full-size CICC [18], this is the first application of the code to a long (∼34 m) CICC.

2. Model description

The main items of the model, namely the distributed parameter electromagnetic model of the cable, the thermal-hydraulic model and their coupling are described in this section. The lumped parameter joint model, implemented in the full version of THELMA, is not needed since we will consider only cases with zero transport current, and therefore it will not be used here or discussed further.

2.1. Electromagnetic cable model

The electromagnetic model of the superconducting (SC) cable in THELMA is based on a distributed parameter circuit approach. The equations of the model are derived from the magneto-quasi-static formulation of the Maxwell equations. The unknowns of the problem are the values of the currents (I_α, with $\alpha = 1, \ldots, N_{CE}$) in each cable element (CE), where N_{CE} is the number of CEs which are utilized to model the SC cable. A CE can be anything from a part of a strand to a strand bundle (e.g., a petal in a full-size ITER CICC). The current in each CE is assumed uniformly distributed in its cross section and is a function of one spatial coordinate (ζ, see figure 1), which is measured along the cable axis line, and of time (t).

The equations describing the current distribution in the CEs are derived from the induction law and have the following form, with index γ, which varies from 1 to ($N_{CE} - 1$):

$$\sum_{\alpha=1}^{N_{CE}} \int_0^L \frac{\partial i_\alpha}{\partial t}(\zeta', t) m_{\gamma,\alpha}(\zeta, \zeta')\, \mathrm{d}\zeta' = -\frac{\partial V_\gamma}{\partial \zeta}(\zeta, t) - E_\gamma\left(\zeta, I_\gamma(\zeta, t), T_\gamma(\zeta, t), B_\gamma(\zeta, t)\right) - \sum_{\beta=1}^{N_{EXT}} \frac{\mathrm{d}I_{EXT,\beta}}{\mathrm{d}t}(t) M_{EXT,\beta,\gamma}(\zeta) - \frac{\mathrm{d}I}{\mathrm{d}t}(t)\, M_{UN,\gamma}(\zeta). \quad (1)$$

In (1), i_α is the difference between I_α and the current in the CE α if a uniform distribution (among the strands of the cable) of the transport current (I) was present[6], L is the length of the cable, $m_{\gamma,\alpha}$ is the induction coefficient per unit length[7] between two infinitesimal portions of CE α and CE γ, respectively, V_γ is the potential of CE γ, E_γ is the tangential component (with respect to the CE axis line) of the electric field in the CE γ, T_γ is the temperature of CE γ, N_{EXT} is the number of external coils, $I_{EXT,\beta}$ is the current in the external coil β, $M_{EXT,\beta,\gamma}$ is the mutual induction coefficient (per unit length) between the external coil β and the CE γ, and $M_{UN,\gamma}$ is the mutual induction coefficient (per unit length) between the whole cable and its CE γ, when the current I is uniformly distributed among the strands[8].

Equation (1) considers the magnetic coupling between each couple of segments of the cable elements. Usually it is not necessary to consider all the magnetic coupling coefficients but a maximum distance (d_{max}) can be defined and magnetic coupling between CE segments, which are at a distance longer than d_{max} apart, can be neglected (thereby reducing the CPU time requirements). The value of d_{max} must be chosen case by case (with a sensitivity analysis) depending on the geometry of the system.

The tangential electric field in the CE (E_γ) is a non-linear function of the current, of the temperature (which is supposed the same for the superconductor and the matrix material) and of the magnetic flux density module (B_γ) in the CE. E_γ is calculated by solving the following equations:

$$I_\gamma = J_{\gamma,sc} A_{\gamma,sc} + J_{\gamma,m} A_{\gamma,m};$$

$$E_\gamma = E_c \left(\frac{|J_{\gamma,sc}|}{J_c(T_\gamma, B_\gamma)}\right)^{n(T_\gamma, B_\gamma)} \times \mathrm{sgn}(J_{\gamma,sc}) = \rho_m(T_\gamma, B_\gamma) J_{\gamma,m} \quad (2)$$

where $A_{\gamma,sc}$ and $A_{\gamma,m}$ are the areas of superconductor and matrix material, respectively, in the cross section of the CE γ, $J_{\gamma,sc}$ and $J_{\gamma,m}$ are the current density in the superconductor

[6] The model equations are derived for the current differences 'i' (instead of the total currents in the cable elements 'I'). Among others, this helps avoiding possible numerical problems that could arise when dealing with small current imbalances.

[7] In the rest of the paper, the induction coefficients, as well as the transverse conductances, are always considered per unit length, unless otherwise specified.

[8] Thanks to the choice of dependent variable 'i', it is possible to split the mutual induction effects into two contributions. The first one represents the mutual induction between the CEs and the cable, if a uniform current distribution among strands was present; this term is a known term because the total transport current is a known quantity. The second one represents the mutual induction between the CEs, which can be neglected when the distance between CEs is large, as explained in the text below.

and in the matrix material, E_c and J_c are the critical parameters of the superconductor, n is the characteristic index of the superconductor and ρ_m is the electrical resistivity of the matrix material. Only $N_{CE} - 1$ equations of type (1) are considered in the model because the current in the last cable element is derived by means of the following equation:

$$i_{N_{CE}}(\zeta, t) = -\sum_{\alpha=1}^{N_{CE}-1} i_\alpha(\zeta, t). \tag{3}$$

The current balance on an infinitesimal length along the generic CE γ gives the relation between the voltages and the spatial derivative of the currents, connected by the transverse conductance matrix (with generic element $g_{\lambda,\gamma}$) in the following equations:

$$\sum_{\lambda=1}^{N_{CE}} g_{\lambda,\gamma}(\zeta, t)\left[V_\lambda(\zeta, t) - V_\gamma(\zeta, t)\right] = \frac{\partial i_\gamma}{\partial \zeta}(\zeta, t) + \sum_{\beta=1}^{N_{EXT}} \frac{dI_{EXT,\beta}}{dt}(t)\left\{\sum_{\lambda=1}^{N_{CE}}\left[g_{\lambda,\gamma}(\zeta, t) M_{EXT,\beta,\lambda,\gamma}(\zeta)\right]\right\} + \frac{dI}{dt}(t)\left\{\sum_{\lambda=1}^{N_{CE}}\left[g_{\lambda,\gamma}(\zeta, t) M_{UN,\lambda,\gamma}(\zeta)\right]\right\} \tag{4}$$

where the index γ varies from 1 to $(N_{CE} - 1)$. $M_{EXT,\beta,\lambda,\gamma}$ and $M_{UN,\lambda,\gamma}$ take into account the magnetic coupling of the external coil β and of the transport current, respectively, with the currents flowing from CE λ to CE γ. The transverse conductances, as well the parameters of the E–J characteristic of the superconductor, must be derived from experimental data on short cable samples. The mutual induction coefficients are calculated numerically once the geometry of the axis line of all cable elements is described.

Equations (4) are utilized to calculate the voltages when the currents in the CEs are known. In matrix notation the equation is the following:

$$\mathbf{V}^*(\zeta, t) = \left(\mathbf{G}^*(\zeta, t)\right)^{-1}\left[\frac{\partial \mathbf{i}^*}{\partial \zeta}(\zeta, t) + \mathbf{S}^*(\zeta, t)\right] \tag{5}$$

where $\mathbf{V}^*$ is the vector of the voltages of the first $(N_{CE} - 1)$ CEs with respect to the last one, $\mathbf{i}^*$ is the vector of the first $(N_{CE} - 1)$ current differences (see above), $\mathbf{G}^*$ is the non-singular reduced transverse conductance matrix with $(N_{CE} - 1)$ rows and $(N_{CE} - 1)$ columns:

$$G^*_{\lambda,\gamma} = g_{\lambda,\gamma} \qquad \text{if } \lambda \neq \gamma, \qquad G^*_{\lambda,\lambda} = -\sum_{\substack{\gamma=1 \\ \gamma\neq\lambda}}^{N_{CE}} g_{\lambda,\gamma} \tag{6}$$

$\mathbf{S}^*$ is the vector accounting for the magnetic coupling through $M_{EXT,\beta,\lambda,\gamma}$ and $M_{UN,\lambda,\gamma}$.

In matrix notation the set of model equations, derived from (1)–(6), is the following:

$$\int_0^L \mathbf{m}^*(\zeta, \zeta')\frac{\partial \mathbf{i}^*}{\partial t}(\zeta', t)\, d\zeta' = -\frac{\partial}{\partial \zeta}\left\{\left(\mathbf{G}^*(\zeta, t)\right)^{-1} \times \left[\frac{\partial \mathbf{i}^*}{\partial \zeta}(\zeta, t) + \mathbf{S}^*(\zeta, t)\right]\right\} - \mathbf{E}^*\left(\zeta, \mathbf{i}^*(\zeta, t), T_{sc}(\zeta, t)\right) - \mathbf{Z}^*(\zeta, t) \tag{7}$$

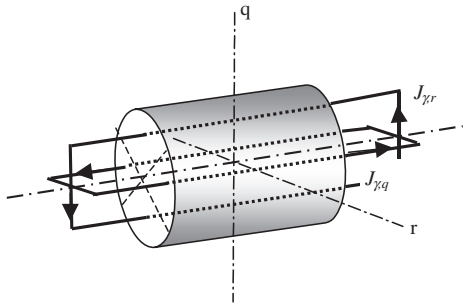

Figure 2. Schematic view of current loops which produce intra-strand losses.

where $\mathbf{m}^*$ is the matrix of the mutual induction coefficient per unit length, $\mathbf{E}^*$ is the vector of the tangential components of the electric field with respect to the CE axes and $\mathbf{Z}^*$ is the vector of the mutual inductances of the CEs with the external coils and with uniformly distributed current.

Once the currents in the first $(N_{CE} - 1)$ CEs are calculated by solving the integral–differential set (7), the current in the N_{CE}th CE is calculated by means of (3) and the $(N_{CE} - 1)$ voltages are calculated by means of (5).

The linear power loss of the cable (P_{loss}) is calculated as split into three terms: the power loss in the SC strands (P_{strand}), the power loss due to coupling currents flowing between different CEs ($P_{inter\text{-}CE}$) and the power loss due to coupling currents flowing inside the CEs ($P_{intra\text{-}CE}$):

$$P_{loss}(\zeta, t) = P_{strand}(\zeta, t) + P_{inter\text{-}CE}(\zeta, t) + P_{intra\text{-}CE}(\zeta, t). \tag{8}$$

The expressions of P_{strand} and $P_{inter\text{-}CE}$ are the following:

$$P_{strand}(\zeta, t) = \sum_{\lambda=1}^{N_{CE}} E_\lambda(\zeta, t) I_\lambda(\zeta, t)\left|\frac{d\mathbf{x}_\lambda(\zeta)}{d\zeta}\right| \tag{9}$$

$$P_{inter\text{-}CE}(\zeta, t) = \sum_{\lambda=1}^{N_{CE}-1}\sum_{\gamma=\lambda+1}^{N_{CE}} g_{\lambda,\gamma}(\zeta, t)\left[V^*_\lambda(\zeta, t) - V^*_\gamma(\zeta, t) - \frac{dI}{dt}(t) M_{UN,\lambda,\gamma}(\zeta) - \sum_{\beta=1}^{N_{EXT}} \frac{dI_{EXT,\beta}}{dt}(t) M_{EXT,\beta,\lambda,\gamma}(\zeta)\right]^2. \tag{10}$$

In (9), the hysteresis component of the losses is neglected. The derivative on the right-hand side accounts for the angle between the CE axis ($\mathbf{x}_\lambda(\zeta)$ is the spatial coordinate of the λth CE axis) and the conductor axis. In (10) the term in the square brackets is related to the electric field component in the cross section of the cable in the direction from the axis of CE λ to the axis of CE γ.

The expression of $P_{intra\text{-}CE}$ is derived by means of a heuristic model. It is supposed that, in each strand of the generic CE γ, the magnetic flux density field, which varies with time, drives current loops circulating between the filaments of the strand. The current loops, which circulate in the cross section of the strand (due to the magnetic field component parallel to the strand axis), are neglected; see figure 2. The magnetic flux density components B_r and B_q in two orthogonal directions, in the cross section of the strand, are

considered and it is supposed that these two components of the field are responsible of two current loops (with currents $\hat{I}_r$ and $\hat{I}_q$), flowing between the filaments of the strand, with a typical dimension of half a twist pitch of the filaments; see figure 2. It is also supposed that these current loops can be described by means of R–L circuits whose parameters have to be obtained from experimental data. With reference to the generic CE γ, the expression of the intra-CE losses is the following:

$$P_{\text{intra-CE},\gamma} = N_{\text{str},\gamma}[b(\hat{I}^2_{\gamma,r} + \hat{I}^2_{\gamma,q}) + \Omega_{+,\gamma}(\hat{I}_{\gamma,r}, I_\gamma) + \Omega_{-,\gamma}(\hat{I}_{\gamma,r}, I_\gamma) + \Omega_{+,\gamma}(\hat{I}_{\gamma,q}, I_\gamma) + \Omega_{-,\gamma}(\hat{I}_{\gamma,q}, I_\gamma)] \tag{11}$$

where $N_{\text{str},\gamma}$ is the number of strands in CE γ, the first term in the square brackets is the linear power loss due current flowing in the transversal direction, and $\Omega_{+,\gamma}$ and $\Omega_{-,\gamma}$ are the non-linear power losses due to current flowing in the longitudinal direction given by

$$\begin{aligned}\Omega_{+,\gamma}(\hat{I}, I) &= \frac{A_{\text{str}}}{4} E\left(\frac{4\hat{I}}{A_{\text{str}}} + \frac{I}{N_{\text{str},\gamma}A_{\text{str}}}\right) \times \left[\frac{4\hat{I}}{A_{\text{str}}} + \frac{I}{N_{\text{str},\gamma}A_{\text{str}}}\right] \\ \Omega_{-,\gamma}(\hat{I}, I) &= \frac{A_{\text{str}}}{4} E\left(\frac{4\hat{I}}{A_{\text{str}}} - \frac{I}{N_{\text{str},\gamma}A_{\text{str}}}\right) \times \left[\frac{4\hat{I}}{A_{\text{str}}} - \frac{I}{N_{\text{str},\gamma}A_{\text{str}}}\right].\end{aligned} \tag{12}$$

The intra-strand coupling currents $\hat{I}_{\gamma,r}$ and $\hat{I}_{\gamma,q}$ are calculated by solving the following R–L circuit equations, once the magnetic flux density terms on the right are known:

$$\begin{aligned}a\frac{\partial \hat{I}_{\gamma,r}}{\partial t}(\zeta,t) + \Psi_\gamma\left(b, \hat{I}_{\gamma,r}(\zeta,t), I_\gamma(\zeta,t)\right) &= c\frac{\partial B_r}{\partial t}(\zeta,t) \\ a\frac{\partial \hat{I}_{\gamma,q}}{\partial t}(\zeta,t) + \Psi_\gamma\left(b, \hat{I}_{\gamma,q}(\zeta,t), I_\gamma(\zeta,t)\right) &= c\frac{\partial B_q}{\partial t}(\zeta,t).\end{aligned} \tag{13}$$

The expression of the resistive terms is:

$$\Psi_\gamma(b, \hat{I}, I) = \left[E\left(\frac{4\hat{I}}{A_{\text{str}}} + \frac{I}{A_{\text{str}}N_{\text{str},\gamma}}\right) + E\left(\frac{4\hat{I}}{A_{\text{str}}} - \frac{I}{A_{\text{str}}N_{\text{str},\gamma}}\right) + b\hat{I}\right]. \tag{14}$$

The model given by equations (11)–(14) depends on three parameters: a, which has the dimension of an inductance per unit length; b, which has the dimension of a resistance per unit length; and c, which has the dimension of a length. These parameters must be obtained from the fit of experimental data on AC losses on short cable samples; see below.

The electromagnetic model just defined still requires initial and boundary conditions: concerning the former, the value of the current in each CE, at any spatial position, must be known at the initial time; concerning the latter, the value of the current at the inlet and outlet sections of each CE shall be imposed at any time.

The discretization of the set of equations (7) is performed by means of linear finite elements in the space coordinate. Taking into account the boundary conditions, a set of first-order ordinary differential equations in time is obtained in the form

$$\mathbf{A}\frac{\mathrm{d}\mathbf{Y}_{\text{em}}}{\mathrm{d}t} = \mathbf{F}(t, \mathbf{Y}_{\text{em}}, \mathbf{T}_{\text{em}}) \tag{15}$$

where $\mathbf{Y}_{\text{em}}$ is a vector whose components are the values of the difference currents at each node of the mesh but the first and the last one, $\mathbf{A}$ is a matrix which takes into account the magnetic coupling between the currents at the nodes of the mesh, $\mathbf{F}$ is a function (possibly non-linear, when near critical conditions in the superconductor are present) taking into account the external magnetic field, the Joule effect and the transverse conductance effects and $\mathbf{T}_{\text{em}}$ is a vector whose components are the temperatures of the conductor in the nodes of the mesh. Equation (15) can be solved by means of a fifth-order Runge–Kutta scheme, or by an implicit scheme based on the trapezoidal rule [19].

2.2. *Thermal-hydraulic model*

An adequate thermal-hydraulic description of the cable is an essential ingredient of the THELMA code. As seen above in (15), some of the terms driving the evolution of the current distribution of the cable depend on the CE temperature distribution $T_\gamma(\zeta, t)$. Therefore, a model is needed, which is able to predict the evolution of the temperature distribution along the cable elements, consistently with the evolution and distribution of the heat sources P_{loss}, computed in turn by the electromagnetic part of the code; see (8) and following. In this respect, the first issue concerns the level of detail that is presumably required to describe the temperature distribution on the cable cross section. For the sake of the present comparison, we assume that the temperature distribution on a given cross section is uniform inside each major cable component, and namely represented on each cross section by only three quantities: T_{sc} (strands), T_{jk} (jacket) and T_{He} (helium). This relatively rough level of detail on the cable cross section is justified because the time scale for equipartition of the temperature inside each cable component on a given cross section is smaller (i.e., faster) than the time scales of interest. For applications to cables where, for example, I_c/T_{CS} transients are studied and/or the use of wrappings naturally identifies the petals as separate flow channels, an extension of this model as discussed in [20] will be needed, including more detail on the conductor cross section.

The thermodynamic state of the helium in the single channel is described by its temperature $T_{\text{He}}(\zeta, t)$ and pressure $p(\zeta, t)$, while the compressible flow of the helium is assumed to occur only in the axial direction, characterized by a single flow speed $v(\zeta, t)$. The set of equations for the five thermal-hydraulic unknowns (T_{sc}, T_{jk}, T_{He}, p, v) is given by the standard set of modified Euler equations for 1D compressible flow of the helium coolant, coupled to 1D conduction equations for the heat transfer along the strands and, separately, along the jacket, as used and validated, for example, in the Mithrandir [21] and M&M [22] codes. Typical boundary conditions for this set are: inlet T_{He}, inlet and outlet p, adiabatic strands and jacket at the cable ends. A first-order finite element discretization in space and a fully implicit scheme with frozen coefficient linearization are used to advance the set in time, for a given value of P_{loss}.

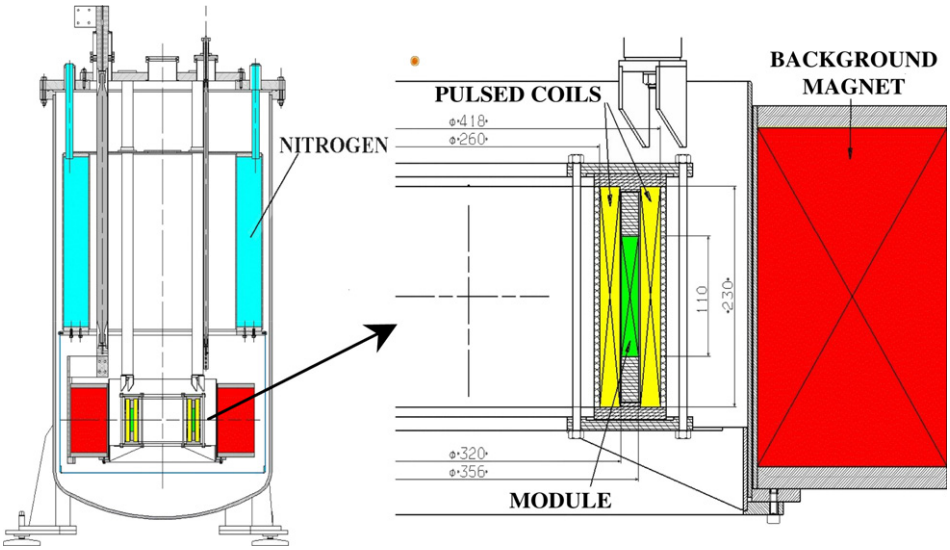

Figure 3. Set-up of the ESE. From the THELMA point of view, the background magnet and the pulsed coils are external (EXT) coils, while the module consists of the different cable elements (CE).

Table 1. Specification of the 12-strand NbTi CICC from the ESE experiment.

Strand manufacturer	Vacuumschmelze
Strand diameter (mm)	0.60
Cu:non-Cu	5.75
Strand coating	Bare
Filament twist pitch (mm)	20
I_c@6 T, 4.2 K (A)	80
Filament diameter (μm)	45
Cable layout	$1 \times 3 \times 4$
Twist pitch of 1st, 2nd stage (mm)	25, 40
Void fraction (%)	40
Conduit inner diameter (mm)	2.68
Conduit outer diameter (mm)	5.18
Conduit material	CuNi
Conductor length (m)	~35
Conductor winding	Double layer

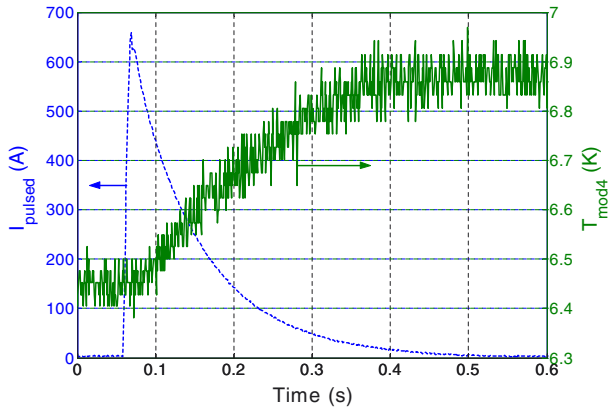

Figure 4. Measured evolution of the current pulse in the pulsed coil (left axis) and of the temperature at T_{mod4} (right axis) for the shot with $\Delta B \sim 0.94$ T and duration 10.8 ms.

2.3. Coupling of electromagnetic and thermal-hydraulic models

The electromagnetic and the thermal-hydraulic models need to be solved simultaneously due to the temperature dependence of the E–J characteristic of the strand. In order to solve the electromagnetic step, the value of $\mathbf{T}_{\mathrm{em}}$ should be known. At the same time, in order to solve the thermal-hydraulic step, the value of the power which is dissipated in the cable elements (P_{loss}) should be known, but this can be calculated only when the value of $\mathbf{Y}_{\mathrm{em}}$ is known. A simple coupling scheme is utilized in the THELMA code: at each time step, first the electromagnetic equations are solved with a constant temperature and P_{loss} is calculated; then the thermal-hydraulic equations are solved using the calculated P_{loss} as a driver, averaged over the time step, and the update of the temperature $\mathbf{T}_{\mathrm{em}}$ is calculated.

3. The ENEA stability experiment (ESE)

A full description of this experiment has already been given elsewhere [23–25]. The main characteristics are briefly summarized in table 1 and the apparatus is sketched in figure 3. The test module is a double-layer solenoid, wound using a sub-size (12 NbTi strands) cable-in-conduit conductor. The simulations of pulsed tests of the ESE were performed with the model described above.

A limited subset of experimental data was selected here. These data were obtained by pulsing with different discharge voltages the capacitor bank supply in order to obtain a fast, homogeneous magnetic field change over the whole conductor length, in the absence of transport current. This change causes a temperature rise in the conductor that could be measured by means of a thermometer (T_{mod4}) positioned along the jacket at a distance of 17.5 m from the conductor inlet. A typical temperature rise as measured by this sensor is shown in figure 4. The deposited energy was evaluated from magnetization measurements [26, 27]. Although it cannot be claimed that this exercise will bring a direct validation of the code capabilities to predict the current distribution, since that was not measured in the ESE, it is still giving some

indirect indication, as the computed current distribution will be used below, together with measured conductances, to assess the AC losses in the conductor and compare them with the measurements.

A subset of the same ESE tests was already analysed using the Gandalf code but this was done from a purely thermal-hydraulic point of view [24]. In that case, due to the lack of an electromagnetic model, the following procedure was used: a uniform power was given as a volumetric heat generation input to the code and parametrically changed in order to match the measured temperature increase. In this way the energy released for each voltage pulse was established. Since, however, the mass flow rate was not accurately measured, an assumption on its value had to be made for the calorimetric assessment of the losses. With the THELMA code a self-consistent procedure can be applied, in which the external magnetic field pulse, calculated from the measured current in the pulsed coil, becomes the major input needed for the code, together with the transverse conductances and the parameters for the $P_{\text{intra-CE}}$ computation from (11), both deduced from tests on short cable samples. An intense characterization activity of short samples of the ESE conductor was indeed done at University of Twente by means of (total) contact resistance measurements and of AC loss measurements. In particular, the transverse conductance between CEs will be obtained from the measured values of the set of contact resistances, see below, and the parameters of the intra-strand loss model will be obtained from the AC loss measurements performed on the short samples.

4. THELMA simulation setup

In order to simulate the experimental results by means of the THELMA code, two different discretizations of the cable cross section have been considered:

(1) Model A, with 12 CEs;
(2) Model B, with 4 CEs.

In the first case, each CE represents a strand of the cable; in the second case each CE represents a triplet of strands. In both models the transverse conductance matrix has the form (16), but the expression of the matrices G_1, G_2 and G_3 is different:

$$G = \begin{bmatrix} G_1 & G_2 & G_3 & G_2 \\ G_2 & G_1 & G_2 & G_3 \\ G_3 & G_2 & G_1 & G_2 \\ G_2 & G_3 & G_2 & G_1 \end{bmatrix}. \tag{16}$$

In model A the following expression is utilized:

$$G_1 = \begin{bmatrix} 0 & g_1 & g_1 \\ g_1 & 0 & g_1 \\ g_1 & g_1 & 0 \end{bmatrix}; \qquad G_2 = \begin{bmatrix} g_2 & g_2 & g_2 \\ g_2 & g_2 & g_2 \\ g_2 & g_2 & g_2 \end{bmatrix}; \qquad G_3 = \begin{bmatrix} g_3 & g_3 & g_3 \\ g_3 & g_3 & g_3 \\ g_3 & g_3 & g_3 \end{bmatrix} \tag{17}$$

where g_1, g_2 and g_3 are the transverse conductances between two strands in the same triplet, two strands in adjacent triplets and two strands in non-adjacent triplets, respectively.

The inter-strand and inter-bundle (i.e., between two triplets) contact resistance (R_c) has been measured at the University of Twente on three conductor samples, having a length of 160 mm each. The measurements are performed at 4.2 K with a four-point-method. The resistance between the selected cable elements is measured at one end of the cable and the other end is cut by electric erosion. Further details of the experimental method can be found in [28] and the results are presented in table 2. Strands numbered from 1 to 3 belong to the same triplet; strands numbered 5 and 6 are from the neighbouring triplet. The other two triplets are used for inter-bundle measurements and are numbered as 7 and 8. It appears that there is an extreme variation in the R_c, in particular between the last-stage bundles. As by experience we know that the spread from sample to sample is typically less than several tens of per cents, while a variation of an order of magnitude is extremely unlikely, we have no clue as to the reasons for the spread of data in table 2. However, based on the database for contact resistance measurements available in Twente, we believe that the values of sample #2 must be considered as being most representative for our conductor.

Table 2. Contact resistance per unit length (R_c) measured on three different ESE conductor short samples: inter-strand (IS) between selected single strands from the first triplet (strand #1, 2, 3) and from the second triplet (strand #5, 6); inter-bundle (IB) between the other two triplets (#7, 8).

Strand combination	Sample #1 R_c (nΩ m)	Sample #2 R_c (nΩ m)	Sample #3 R_c (nΩ m)
1 and 2, IS	171	67	119
1 and 3, IS	191	78	
2 and 3, IS	191	75	
5 and 6, IS	440	58	
1 and 5, IS	1290	55	
1 and 6, IS	1010	121	
2 and 5, IS	1260	121	
7 and 8, IB	1780	124	1500

The values of g_1 (6.00×10^6 S m^{-1}), g_2 (1.78×10^6 S m^{-1}), and g_3 (0 S m^{-1}), have been obtained by fitting the experimental contact resistance measurements reported in table 2 (the calculated value of R_c is ~68 nΩ m between strands of the same triplet, ~93 nΩ m between strands of adjacent triplets and ~109 nΩ m between strands of non-adjacent triplets).

In model B, the only element of the transverse conductance matrix which is different from zero ($g = G_2, G_1 = G_3 = 0$) refers to adjacent triplets. Its value could be deduced in two different ways. Coherently with the values utilized in model A, one should have $g = 9g_2$, since each strand of a triplet has the same conductance g_2 with each strand of an adjacent triplet, thus $g \sim 1.602 \times 10^7$ S m^{-1} is obtained.

Alternatively, the value of g can be calculated in order to fit the data on inter-bundle R_c given in table 2. This can be performed, under the assumptions of:

(a) constant transverse conductance between CEs along the cable length,
(b) the same value of transverse conductance between adjacent CEs,
(c) transverse conductance between non-adjacent CEs equal to zero.

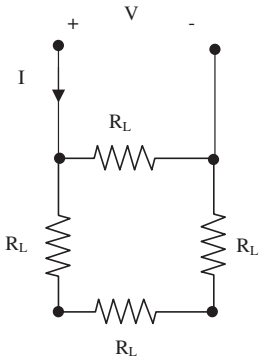

Figure 5. Equivalent electric network used to compute the transverse conductances between CEs when model B is adopted.

From the circuit in figure 5, the set of equations (18) can be deduced:

$$\left.\begin{aligned} R_c^* &= \frac{V}{I} = \frac{3R_L}{4} \\ R_L &= \frac{1}{gL} \end{aligned}\right\} \Rightarrow g = \frac{3}{4LR_c^*} \qquad (18)$$

where L is the length of the cable sample, R_c^* is the measured value of the contact resistance and g is the transverse conductance between CEs, resulting in a maximum value of $g \sim 0.605 \times 10^7$ S m^{-1}. The two approaches give somewhat different results and neither is fully reliable in view of the above-mentioned issues related to the spread of values in table 2. Thus a weighted average $g = 0.8 \times 10^7$ S m^{-1} was used in the following computations, more weight being given to the latter estimate of g, 0.605×10^7 S m^{-1}, in view of its direct experimental origin. With this value, the calculated value of the contact resistance between two adjacent triplets, is ~93.8 nΩ m.

In order to simulate the intra-strand coupling losses with THELMA, the heuristic model, which was described above, has been used[9], freezing the free parameters of the model based on the analysis of the AC loss results on short samples[10]; see appendix A.

With reference to model A, the values of the parameters a (1×10^{-7} H m^{-1}), b (3.77×10^{-6} Ω m^{-1}) and c (1.68×10^{-4} m) were obtained (see figure 6), while for model B, $a = 2.39 \times 10^{-7}$ H m^{-1}, $b = 9.00 \times 10^{-6}$ Ω m^{-1} and $c = 2.64 \times 10^{-4}$ m were obtained. Both models are able to correctly simulate the AC loss results on short samples, thus it is more convenient for the simulations to adopt model B, which is much less CPU-time consuming.

A first assessment of the THELMA code for the simulation of the ESE was performed against the CUDI-CICC code with reference to short conductor samples. Selected results of this exercise are reported in appendix B.

[9] Another possibility is to model the filaments in the strands by considering a certain number of CEs to represent a single strand. The linear power loss computed with this model was compared to that computed with model B, showing a reasonable agreement.

[10] In practice, only two ratios (a/c, b/a) between the three free parameters could be fixed by the analysis of AC losses, since they are in the linear regime; the third parameter could be fixed by a calibration on a single shot of the ESE simulations.

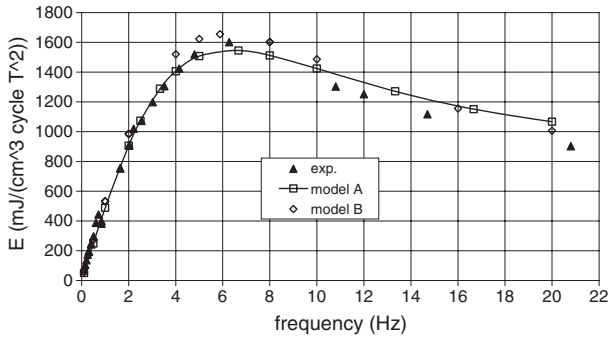

Figure 6. Calculated AC losses ($E = \frac{Q_{\text{cycle}}}{V B_a^2}$) when a 22 cm long cable sample and sinusoidal external magnetic field with amplitude B_a is considered ($B_{dc} = 0$), compared to experimental data. Model A = 12 CEs, model B = 4 CEs; see text.

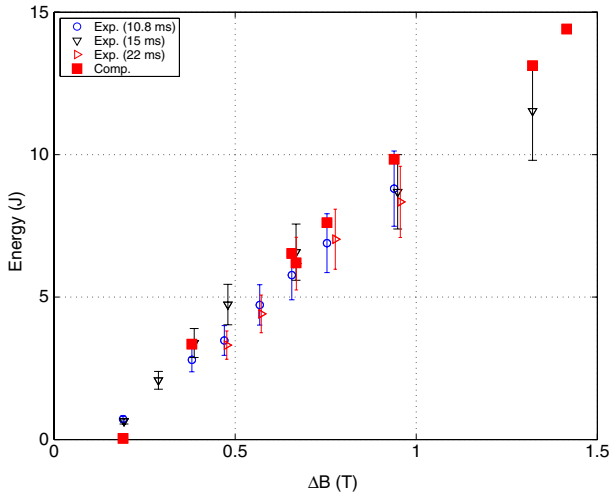

Figure 7. Experimental (open symbols) [26] and computed (full squares) deposited energy as a function of the pulsed field. For the point at highest ΔB, the experimental evaluation of the energy is missing.

The ESE runs, which were used for the THELMA simulations, refer to different field rates, in the range 1–130 T s^{-1}; thus, both inter- and intra-strand loss mechanisms must be well modelled in order to reproduce the experimental results (see also appendix B). The simulation of ESE runs with peak external voltage variable from 700 to 1500 V was performed. In order to guarantee spatial convergence, a mesh with 5 nodes per twist pitch length was utilized (uniform grid with 4274 elements)[11]. The scaling given in [23] for the filament J_c was used with the following values of the parameters: $T_{c0} = 9.2$ K, $B_{c20} = 14.5$ T, $\alpha = 0.8$, $\beta = 0.8$, $\gamma = 2.45$, $\delta = 1.7$, $C_0 = 7.45 \times 10^{10}$ A m^{-2} T. Simulations started from stationary thermal-hydraulic conditions with inlet pressure and temperature respectively of 9.6 bar and 6.5 K respectively, assuming a mass flow rate $dm/dt \sim 0.3$ g s^{-1}.

5. Results and discussion

Figure 7 shows the calculated energy dissipated in the conductor versus the magnetic field pulse amplitude, which

[11] A more refined mesh, with ~7000 nodes, should be used to guarantee convergence with model A.

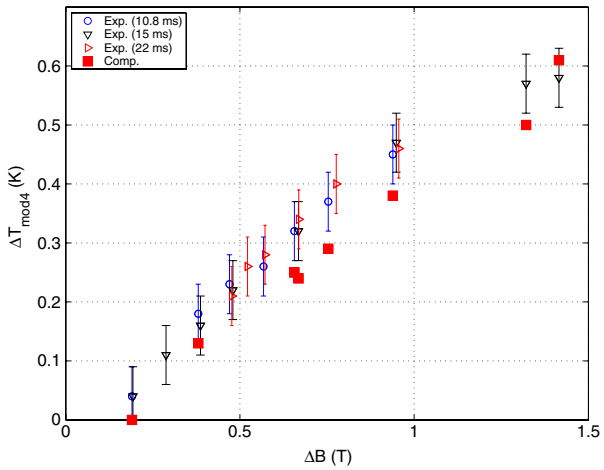

Figure 8. Experimental (open symbols) and computed (full squares) maximum T_{mod4} increase in time as a function of the pulsed field.

is compared to the measured one [26, 27]. The experimental values of ΔT_{mod4}, i.e., the maximum increase of T_{mod4}, are reported in figure 8, together with the experimental error bars coming from the disturbance of the measured signal; see also figure 4. With respect to the experimental evolution, see figure 4, the calculated time evolution of the jacket temperature is faster (see below); the maximum is reached in the calculation about 100 ms after the start of the pulsed field, while in the experimental data the maximum is reached after about 400 ms. This discrepancy may be explained observing that the data acquisition system gives, during fast transients, a delay between the actual jacket temperature and the measured temperature [29], so that only the maximum temperature *increase* ΔT_{mod4} at the sensor is considered for the comparison with the computations.

The measured deposited energy scales $\sim$ linearly with ΔB, which was explained in [25] as being related to saturation effects occurring in the cable, with the coupling currents reaching the critical current I_{c} in some of the filaments. This induces a similar dependence of the measured temperature increase ΔT_{mod4} on ΔB. The experimental behaviour is well reproduced by THELMA, see figures 7 and 8, with an agreement typically close to the experimental error bars. Indeed, the simulations presented here confirm that the Joule dissipation in the SC filaments (equation (9) and non-linear terms in equation (11)) is typically larger (about twice) than the total coupling losses (equation (10) and linear terms in equation (11)).

The computed evolution of the thermal-hydraulic driver, i.e., the power deposited in the strands due to the AC losses, for the pulse with $\Delta B \sim 0.94$ T and duration 10.8 ms, is reported in figure 9(a), together with the temperature evolution of the different conductor components at the location of T_{mod4} (figure 9(b)). The shape of the deposited power follows the shape of the computed pulsed current derivative (not shown), obtained from the experimental current evolution, and this explains the irregular evolution. The current ramp-up is faster than the ramp-down (see figure 4), leading to a far more intense heat deposition during the first part of the transient (up to 10.8 ms). The peak value of the deposited power corresponds to the phase of the ramp-up with the maximum slope, at $\sim$1–2 ms from the beginning of the pulse. Since in the simulation the power is deposited directly into the strands, the strand temperature is the first to react, followed by the helium, which cools the strands, and by the jacket, which is heated by the helium and, for a certain fraction, directly by the contact with the strands.

The power loss, as well as the temperature increase, has been calculated above from the current distribution. The latter, computed for example 4 ms after the pulse start-up in the same simulation to which figure 9 refers, is shown for the sake of completeness in figure 10, with reference to the sector of the cable with axial coordinate between 2.0 and 2.2 m.

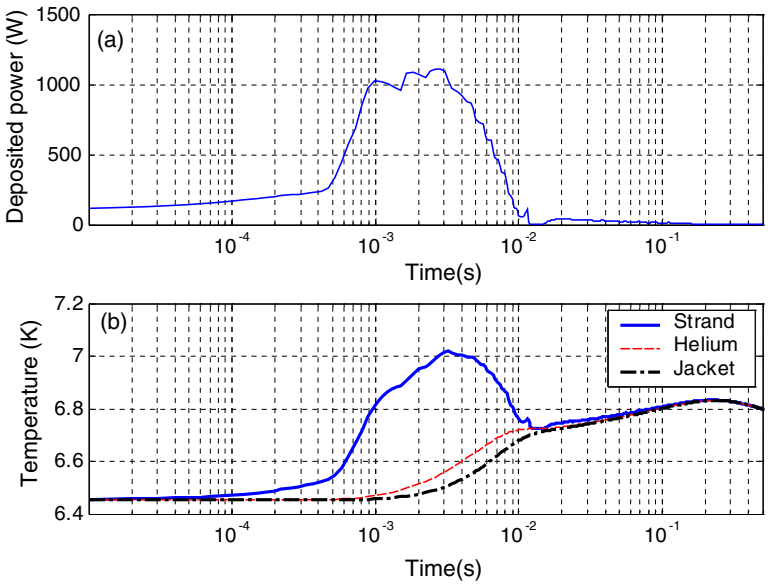

Figure 9. Shot with $\Delta B \sim 0.94$ T and duration 10.8 ms. (a) Evolution of the computed power deposited in the strands. (b) Computed temperature evolution of the strands (solid), helium (dashed) and jacket (dash–dotted) at the location of T_{mod4} during and after the pulse (the AC pulse begins at $t = 0$ s).

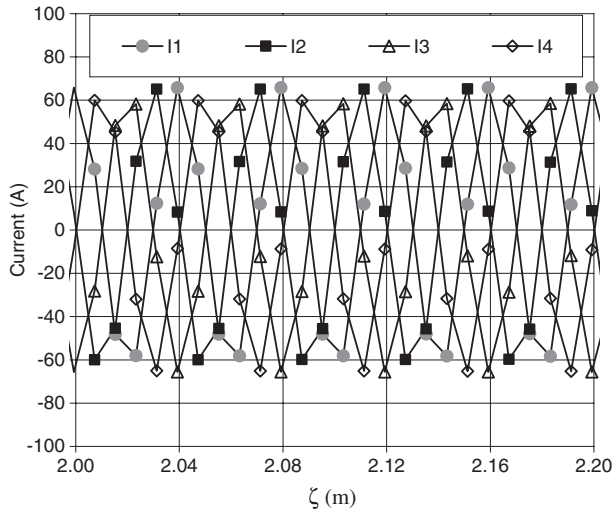

Figure 10. Current distribution along a small portion of the cable, 4 ms after the pulse start—in the shot with $\Delta B \sim 0.94$ T and duration 10.8 ms.

The picture shows that current loops (at zero total transport current) develop between the CEs over half a twist pitch length (0.04 m). This current distribution is representative of the behaviour over most of the cable, except in the end and in the middle sections, which correspond to the coil boundaries. This is connected to the distribution of the magnetic flux density along the cable, which is the only electro-motive force present in the experiment. The total field (not shown) is the superposition of the external pulsed coil field, which is practically uniform along the cable elements, and of the self-field, which has significant variations only in correspondence of the upper and lower ends of the coil.

6. Conclusions

The electro-magnetic cable model included in the THELMA code has been presented in detail for the first time, together with the thermal-hydraulic model and their coupling. The code has then been used to simulate the pulsed runs of the ESE database.

Different discretizations of the cable cross section have been utilized, based on either 4 or 12 CEs, each CE representing either a triplet of strands or a single strand, respectively. As it is crucial to include the generation of intra-strand coupling loss in the overall computation, these have been simulated with an approximate but not too CPU-time consuming model. The input data for the THELMA code (transverse conductance between CEs and intra-strand coupling loss parameters) have been obtained by best fitting contact resistance R_c and AC loss experimental data, which were measured on short samples of the cable at the University of Twente.

Some experimental runs of the ESE, with pulsed magnetic field of different amplitudes and durations, were simulated.

The results show that it is possible to adopt an approximate model (4 CEs) for AC losses in the cable, with parameters based on the experimental short-sample data, when real-size systems are considered, leading to a significant improvement in the CPU time requirements.

Although it cannot be claimed that this work gives a *direct* validation of the THELMA code capabilities to predict the current distribution, since the latter was not measured in the ESE, it does so *indirectly*, as the computed current distribution is used to assess the AC losses in the conductor. These show good agreement with the measurements, with reference to both the deposited energy and the maximum increase of jacket temperature.

Acknowledgments

This work was partially financially supported by the European Fusion Development Agreement (EFDA) and by the Italian Ministry for Education, University and Research (MIUR). We should also like to thank one of the anonymous referees for the careful reading and constructive criticism, which significantly improved the readability of the paper.

Appendix A. AC loss measurements on ESE conductor short samples

The AC loss of ESE conductor short samples was determined in a calorimetric way on a bundle of 15 sections, each 220 mm long. The conductors were subjected to sinusoidal field changes in a broad frequency range from 0.01 to 20 Hz. The experimental results are reported in figures 6 and A.1, and they show that the AC loss versus the frequency of the applied field from the ESE conductor can apparently be described with the commonly used single time constant model and that the coupling current loss per unit volume goes with the square of the applied AC field amplitude, B_a^2. The coupling loss time constants found for both amplitudes of $B_a = 200$ and 400 mT, with $B_{dc} = 0$ T, both amount to $n\tau = 42$ ms. The penetration field is determined by means of the field dependent critical current density $J_c(B)$ relation combined with the filament diameter (45 μm) and from the hysteresis loss extrapolations in the AC loss curves at 200 and 400 mT amplitudes, giving good agreement. The penetration field amounts to $B_p = 240$ mT. This means that for $B_a < B_p$, no full penetration occurs and this may lead to some underestimation of the AC loss at the lower amplitudes (and higher frequencies) for the data in figure 6. The experimental conditions did not allow for a combination of higher frequencies and high B_a.

The experimentally determined coupling loss time constant ($n\tau$) is an overall $n\tau$, which contains the intra-strand coupling loss (filament coupling and matrix eddy currents), the inter-strand coupling loss, the eddy current loss generated in the CuNi conduit and the coupling between conduit and cable. The contribution to time constant of eddy currents was calculated as described in [30] and resulted in being negligible with respect to the experimental value. The level of inter-strand (IS) R_c, in combination with the number of strands, gives a rather effective indication of the inter-strand coupling loss time constant of a CICC [28, 31, 32].

By using the results of a database available in Twente, obtained on various CICCs, it becomes clear that, with the present relatively high level of IS R_c (100 nΩ m), the inter-strand $n\tau$ is expected to be in the range of only a few ms, which is far below the measured value of ~42 ms for the conductor. From the value of the twist pitch of the SC filaments in the

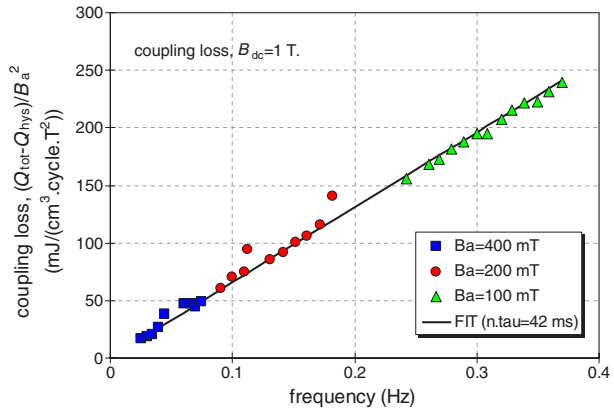

Figure A.1. Normalized conductor coupling loss versus frequency for different amplitudes of the applied pulsed field $B_a = 100$, 200 and 400 mT, and $B_{dc} = 1$ T.

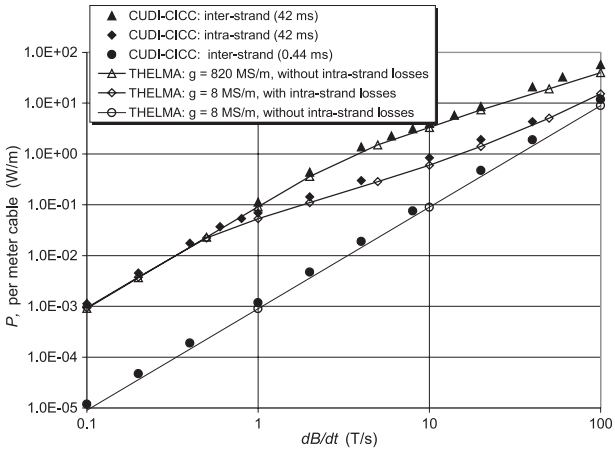

Figure B.1. The coupling loss per metre length simulated with CUDI-CICC and THELMA as produced by a 200 mm cable versus the applied dB/dt with $T = 6.5$ K and $B_{dc} = 2.7$ T.

strand a first estimate of the coupling loss time constant for a strand can be calculated [28]. The twist pitch of the strand has been determined as ∼20 mm (±10%) on two different strand sections taken from different cabling stages of the same piece of conductor. The outer copper shell was removed with a solution of HNO_3 and the filament twist was checked under a microscope. Scaling the $n\tau$ for the ESE strand as with the data from [28], for a twist pitch of 20 mm an $n\tau$ of ∼39 ms was obtained. It can then be concluded that, due to the combination of relatively long filament twist pitch and high inter-strand R_c, the main loss mechanism at low frequency should be the intra-strand coupling currents.

Appendix B. Comparisons with CUDI-CICC

As a complete description of CUDI-CICC can be found in [10, 14], only the characteristics of the code which are relevant for the comparison with THELMA are briefly reviewed in this paper. CUDI-CICC is a dynamic code that solves the Kirchhoff lumped parameters circuit equations using an implicit time stepping method. The network mesh handles one cable stage and so the cable is divided into N_s subunits each representing one sub-cable. In the case of the ESE simulation, four sub-cables (triplets) are considered and represented by lines with infinitely small diameter and twist pitch $L_{p,s} = 40$ mm, which equals the pitch of the last stage. The sub-cables are represented by resistances R_s and inductances L_s, connected in series, with interconnection resistances R_a. Transverse resistances R_a between the cable bundles are derived from directly measured values. The series resistance R_s simulates current sharing from superconducting filaments to normal conducting stabilizer due to current saturation. After a length $L_b = L_{p,s}/N_s$ the geometrical configuration is repeated periodically and such a cable section with length L_b is called a band. For comparison with THELMA a short 200 mm section of the cable was considered, corresponding to $N_b = 20$ bands in the CUDI-CICC model.

The comparison between THELMA and CUDI-CICC was done with reference to current saturation of the coupling loss in a cable and in a strand. At very high field rates, inter-strand coupling currents can locally reach the critical current of single strands in the cable, and intra-strand coupling currents can locally reach the critical current of single filaments in the strands. A different behaviour is expected in the two cases and it was studied by both codes. The pure inter-strand loss was calculated by CUDI-CICC with a four-element model of the cable but with two different values of the transverse resistance R_a: (1) $R_a = 12.7$ μΩ leading to $n\tau \sim 0.44$ ms and (2) $R_a = 0.127$ μΩ leading to $n\tau \sim 42$ ms. The same case was analysed by THELMA with model B, neglecting intra-strand losses, with two different values of the transverse conductivity: (1) $g = 8 \times 10^6$ S m^{-1}, leading to $n\tau \sim 0.44$ ms and (2) $g = 8.2 \times 10^8$ S m^{-1}, leading to $n\tau \sim 42$ ms.

The real case, with high intra-strand losses, was calculated: by CUDI-CICC, with a four-filament model of a strand with an outer diameter of 0.5 mm and a pitch of 20 mm; by THELMA, with model B with $g = 8 \times 10^6$ S m^{-1} and intra-strand coupling losses ($a = 2.39 \times 10^{-7}$ H m^{-1}, $b = 9.00 \times 10^{-6}$ Ω m^{-1}, $c = 2.64 \times 10^{-4}$ m). A short 200 mm sample of the cable, as previously described, subject to a uniform magnetic field rate dB/dt was considered for the calculations; the temperature was 6.5 K and the critical current density of the superconductor was assumed to be 1.23×10^9 A m^{-2}, independent of the magnetic field amplitude, corresponding to a magnetic field of 2.7 T.

The calculated power losses versus the field rate are reported in figure B.1. A good agreement between the results of the two codes was obtained. The figure shows that below $dB/dt \sim 1$ T s^{-1} the intra-strand loss is dominant, while at increasing dB/dt the inter-strand component becomes more and more important. The reason for this is the saturation of the intra-strand loss when exceeding ∼1 T s^{-1}.

References

[1] Martovetsky N N 2004 ITER Model coil test overview: Nb3Sn strand properties in cable-in conduit conductors *Physica* C **401** 22–7

[2] Mitchell N 2003 Summary, assessment and implications of the ITER model coil test results *Fusion Eng. Des.* **66–68** 971–93

[3] Bruzzone P *et al* 2005 Test results of the ITER PF insert conductor short sample in SULTAN *IEEE Trans. Appl. Supercond.* **15** 1351–4

[4] Ciazynski D, Zani L, Gislon P, Muzzi L, Bruzzone P, Wesche R, Stepanov B, Zapretilina E, Martovetsky N and Bessette D 2005 DC performances of ITER NbTi conductors: models vs measurements *IEEE Trans. Appl. Supercond.* **15** 1355–8

[5] Zanino R, Mitchell N and Savoldi Richard L 2003 Analysis and interpretation of the full set (2000-2002) of Tcs tests in conductor 1A of the ITER central solenoid model coil *Cryogenics* **43** 179–97

[6] Zanino R and Savoldi Richard L 2003 Performance evaluation of the ITER toroidal field model coil phase I. Part 2: M&M analysis and interpretation *Cryogenics* **43** 91–100

[7] Zanino R *et al* 2004 Tcs tests and performance assessment of the ITER toroidal field model coil (Phase II) *IEEE Trans. Appl. Supercond.* **14** 1519–22

[8] Verweij A P 1995 Electrodynamics of superconductor cables in accelerator magnets *Thesis* University of Twente, ISBN 90-9008555-6

[9] Akhmetov A 1998 Network models of superconducting cables and the results of the matrix approach to their description *Physica* C **310** 309–15

[10] Nijhuis A, Knoopers H G, ten Haken B and ten Kate H H J 2000 Model study on AC loss and current distribution in a superconducting multi strand cable *Report UT-NET 2000-1* Faculty of Applied Physics, University of Twente, The Netherlands

[11] Ciazynski D and Duchateau J L 2001 Validation of the CEA electrical network model for the ITER coils *IEEE Trans. Appl. Supercond.* **11** 1530–3

[12] Meinecke C, Miri A M and Petranovic R 2001 Numerical investigation of the current distribution in cable in conduit conductors using lumped network models *IEEE Trans. Appl. Supercond.* **11** 2579–82

[13] Bellina F, Boso D, Schrefler B A and Zavarise G 2002 Modeling a multistrand SC cable with an electrical DC lumped network *IEEE Trans. Appl. Supercond.* **12** 1408–12

[14] Nijhuis A, Knoopers H G, Ilyin Y, Godeke A, ten Haken B and ten Kate H H J 2002 Effect of self-field and current non-uniformity on the voltage–temperature characteristic of the ITER central solenoid insert coil by numerical calculations *Cryogenics* **42** 469–83

[15] Mitchell N 2000 Modelling of non-uniform current diffusion coupled with thermohydraulic effects in superconducting cables *Cryogenics* **40** 637–53

[16] Akhmetov A, Bottura L and Breschi M 2001 A continuum model for current distribution in Rutherford cables *IEEE Trans. Appl. Supercond.* **11** 2138–41

[17] Bottura L, Rosso C and Breschi M 2000 A general model for thermal, hydraulic and electric analysis of superconducting cables *Cryogenics* **40** 617–26

[18] Zanino R, Bagnasco M, Bellina F, Gislon P, Ribani P L and Savoldi Richard L 2005 Modeling AC losses in the ITER NbTi poloidal field full size joint sample (PF-FSJS) using the THELMA code *Fusion Eng. Des.* C **75–79** 23–7

[19] Press W H, Teukolsky S A, Vetterling W T and Flannery B P 2001 *Numerical Recipes in Fortran 77: The Art of Scientific Computing* 2nd edn (Cambridge: Cambridge University Press)

[20] Zanino R *et al* 2006 Implications of NbTi short-sample test results and analysis for the ITER poloidal field conductor insert (PFCI) *IEEE Trans. Appl. Supercond.* **16** 886–9

[21] Zanino R, De Palo S and Bottura L 1995 A two-fluid code for the thermohydraulic transient analysis of CICC superconducting magnets *J. Fusion Energy* **14** 25–40

[22] Savoldi L and Zanino R 2000 Thermal-hydraulic analysis of Tcs measurement in conductor 1A of the ITER central solenoid model coil using the M&M code *Cryogenics* **40** 593–604

[23] Bottura L *et al* 2001 Stability in a long length NbTi CICC *IEEE Trans. Appl. Supercond.* **11** 1542–5

[24] Bellucci P, Ciotti M, Gislon P, Spadoni M, Bottura L, Muzzi L and Turtù S 2000 Comparison between the predictions of the thermo-hydraulic code Gandalf and the results of a long length instrumented CICC module experiment *Cryogenics* **40** 555–9

[25] Ciotti M, Di Zenobio A, Gislon P, Muzzi L, Spadoni M and Turtù S 2002 Loss calculations in a CICC solenoid exposed to rapidly changing magnetic fields *Physica* C **372–376** 1750–3

[26] Muzzi L, Gislon P, Turtù S and Spadoni M 2003 Inductive heating on a NbTi CICC magnet: energy calibration and stability analysis *Cryogenics* **43** 699–704

[27] Muzzi L and Spadoni M 2003 Magnetic method for AC losses measurement of coil wound CICCs in pulsed regimes *Supercond. Sci. Technol.* **16** 19–23

[28] Nijhuis A, ten Kate H H J, Duchateau J and Decool P 2001 Control of contact resistance by strand surface coating in 36-strand NbTi CICCs *Cryogenics* **41** 1–7

[29] Gislon P 2003 private communication

[30] Namjoshi K V and Biringer P P 1988 Low-frequency eddy current loss estimation in long conductors by using the moment of inertia of cross sections *IEEE Trans. Magn.* **24** 2181–5

[31] Nijhuis A, ten Kate H H J, Bruzzone P and Bottura L 1996 Parametric study on coupling loss in sub-size ITER Nb3Sn cabled specimen *IEEE Trans. Magn.* **32** 2743–6

[32] Nijhuis A and ten Kate H H J 2000 Surface oxidation and interstrand contact resistance of Cr-coated Nb3Sn and bare NbTi strands in CICC's *Adv. Cryog. Eng.* B **46** 1083–90